Physics Letters B 791 (2019) 375–384

Contents lists available at ScienceDirect

Physics Letters B

www.elsevier.com/locate/physletb

Measurement of the phase between strong and electromagnetic amplitudes of J/ψ decays

BESIII Collaboration

M. Ablikim [a], M.N. Achasov [i,4], S. Ahmed [n], M. Albrecht [d], A. Amoroso [bf,bh], F.F. An [a], Q. An [bc,ap], Y. Bai [ao], O. Bakina [z], R. Baldini Ferroli [t], Y. Ban [ah], D.W. Bennett [s], J.V. Bennett [e], N. Berger [y], M. Bertani [t], D. Bettoni [v], J.M. Bian [az], F. Bianchi [bf,bh], E. Boger [z,2], I. Boyko [z], R.A. Briere [e], H. Cai [bj], X. Cai [a,ap], O. Cakir [as], A. Calcaterra [t], G.F. Cao [a,aw], S.A. Cetin [at], J. Chai [bh], J.F. Chang [a,ap], G. Chelkov [z,2,3], G. Chen [a], H.S. Chen [a,aw], J.C. Chen [a], M.L. Chen [a,ap], P.L. Chen [bd], S.J. Chen [af], X.R. Chen [ac], Y.B. Chen [a,ap], X.K. Chu [ah], G. Cibinetto [v], H.L. Dai [a,ap], J.P. Dai [ak,8], A. Dbeyssi [n], D. Dedovich [z], Z.Y. Deng [a], A. Denig [y], I. Denysenko [z], M. Destefanis [bf,bh], F. De Mori [bf,bh], Y. Ding [ad], C. Dong [ag], J. Dong [a,ap], L.Y. Dong [a,aw], M.Y. Dong [a,ap,aw], Z.L. Dou [af], S.X. Du [bl], P.F. Duan [a], J. Fang [a,ap], S.S. Fang [a,aw], X. Fang [bc,ap], Y. Fang [a], R. Farinelli [v,w], L. Fava [bg,bh], S. Fegan [y], F. Feldbauer [y], G. Felici [t], C.Q. Feng [bc,ap], E. Fioravanti [v], M. Fritsch [y,n], C.D. Fu [a], Q. Gao [a], X.L. Gao [bc,ap], Y. Gao [ar], Y.G. Gao [f], Z. Gao [bc,ap], I. Garzia [v], K. Goetzen [j], L. Gong [ag], W.X. Gong [a,ap], W. Gradl [y], M. Greco [bf,bh], M.H. Gu [a,ap], S. Gu [o], Y.T. Gu [l], A.Q. Guo [a], L.B. Guo [ae], R.P. Guo [a,aw], Y.P. Guo [y], Z. Haddadi [ab], S. Han [bj], X.Q. Hao [o], F.A. Harris [ax], K.L. He [a,aw], F.H. Heinsius [d], T. Held [d], Y.K. Heng [a,ap,aw], T. Holtmann [d], Z.L. Hou [a], C. Hu [ae], H.M. Hu [a,aw], T. Hu [a,ap,aw], Y. Hu [a], G.S. Huang [bc,ap], J.S. Huang [o], X.T. Huang [aj], X.Z. Huang [af], Z.L. Huang [ad], T. Hussain [be], W. Ikegami Andersson [bi], Q. Ji [a], Q.P. Ji [o], X.B. Ji [a,aw], X.L. Ji [a,ap], X.S. Jiang [a,ap,aw], X.Y. Jiang [ag], J.B. Jiao [aj], Z. Jiao [q], D.P. Jin [a,ap,aw], S. Jin [a,aw], Y. Jin [ay], T. Johansson [bi], A. Julin [az], N. Kalantar-Nayestanaki [ab], X.L. Kang [a], X.S. Kang [ag], M. Kavatsyuk [ab], B.C. Ke [e], T. Khan [bc,ap], A. Khoukaz [ba], P. Kiese [y], R. Kliemt [j], L. Koch [aa], O.B. Kolcu [at,6], B. Kopf [d], M. Kornicer [ax], M. Kuemmel [d], M. Kuessner [d], M. Kuhlmann [d], A. Kupsc [bi], W. Kühn [aa], J.S. Lange [aa], M. Lara [s], P. Larin [n], L. Lavezzi [bh], S. Leiber [d], H. Leithoff [y], C. Leng [bh], C. Li [bi], Cheng Li [bc,ap], D.M. Li [bl], F. Li [a,ap], F.Y. Li [ah], G. Li [a], H.B. Li [a,aw], H.J. Li [a,aw], J.C. Li [a], K.J. Li [aq], Kang Li [m], Ke Li [aj], Lei Li [c], P.L. Li [bc,ap], P.R. Li [aw,g], Q.Y. Li [aj], T. Li [aj], W.D. Li [a,aw], W.G. Li [a], X.L. Li [aj], X.N. Li [a,ap], X.Q. Li [ag], Z.B. Li [aq], H. Liang [bc,ap], Y.F. Liang [am], Y.T. Liang [aa], G.R. Liao [k], D.X. Lin [n], B. Liu [ak,8], B.J. Liu [a], C.X. Liu [a], D. Liu [bc,ap], F.H. Liu [al], Fang Liu [a], Feng Liu [f], H.B. Liu [l], H.M. Liu [a,aw], Huanhuan Liu [a], Huihui Liu [p], J.B. Liu [bc,ap], J.P. Liu [bj], J.Y. Liu [a,aw], K. Liu [ar], K.Y. Liu [ad], Ke Liu [f], L.D. Liu [ah], P.L. Liu [a,ap], Q. Liu [aw], S.B. Liu [bc,ap], X. Liu [ac], Y.B. Liu [ag], Z.A. Liu [a,ap,aw], Zhiqing Liu [y], Y.F. Long [ah], X.C. Lou [a,ap,aw], H.J. Lu [q], J.G. Lu [a,ap], Y. Lu [a], Y.P. Lu [a,ap], C.L. Luo [ae], M.X. Luo [bk], X.L. Luo [a,ap], X.R. Lyu [aw], F.C. Ma [ad], H.L. Ma [a], L.L. Ma [aj], M.M. Ma [a,aw], Q.M. Ma [a], T. Ma [a], X.N. Ma [ag], X.Y. Ma [a,ap], Y.M. Ma [aj], F.E. Maas [n], M. Maggiora [bf,bh], Q.A. Malik [be], Y.J. Mao [ah], Z.P. Mao [a], S. Marcello [bf,bh], Z.X. Meng [ay], J.G. Messchendorp [ab], G. Mezzadri [v], J. Min [a,ap], T.J. Min [a], R.E. Mitchell [s], X.H. Mo [a,ap,aw], Y.J. Mo [f], C. Morales Morales [n], G. Morello [t], N.Yu. Muchnoi [i,4], H. Muramatsu [az], A. Mustafa [d], Y. Nefedov [z], F. Nerling [j,7], I.B. Nikolaev [i,4], Z. Ning [a,ap], S. Nisar [h], S.L. Niu [a,ap], X.Y. Niu [a,aw], S.L. Olsen [ai,10], Q. Ouyang [a,ap,aw], S. Pacetti [u], Y. Pan [bc,ap], M. Papenbrock [bi],

https://doi.org/10.1016/j.physletb.2019.03.001

P. Patteri [t], M. Pelizaeus [d], J. Pellegrino [bf,bh], H.P. Peng [bc,ap], K. Peters [j,7], J. Pettersson [bi], J.L. Ping [ae], R.G. Ping [a,aw], A. Pitka [y], R. Poling [az], V. Prasad [bc,ap], H.R. Qi [b], M. Qi [af], S. Qian [a,ap], C.F. Qiao [aw], N. Qin [bj], X.S. Qin [d], Z.H. Qin [a,ap], J.F. Qiu [a], K.H. Rashid [be,9], C.F. Redmer [y], M. Richter [d], M. Ripka [y], M. Rolo [bh], G. Rong [a,aw], Ch. Rosner [n], X.D. Ruan [l], A. Sarantsev [z,5], M. Savrié [w], C. Schnier [d], K. Schoenning [bi], W. Shan [ah], M. Shao [bc,ap], C.P. Shen [b], P.X. Shen [ag], X.Y. Shen [a,aw], H.Y. Sheng [a], J.J. Song [aj], W.M. Song [aj], X.Y. Song [a], S. Sosio [bf,bh], C. Sowa [d], S. Spataro [bf,bh], G.X. Sun [a], J.F. Sun [o], L. Sun [bj], S.S. Sun [a,aw], X.H. Sun [a], Y.J. Sun [bc,ap], Y.K. Sun [bc,ap], Y.Z. Sun [a], Z.J. Sun [a,ap], Z.T. Sun [s], C.J. Tang [am], G.Y. Tang [a], X. Tang [a], I. Tapan [au], M. Tiemens [ab], B. Tsednee [x], I. Uman [av], G.S. Varner [ax], B. Wang [a], B.L. Wang [aw], D. Wang [ah], D.Y. Wang [ah], Dan Wang [aw], K. Wang [a,ap], L.L. Wang [a], L.S. Wang [a], M. Wang [aj], Meng Wang [a,aw], P. Wang [a], P.L. Wang [a], W.P. Wang [bc,ap], X.F. Wang [ar], Y. Wang [an], Y.D. Wang [n,*], Y.F. Wang [a,ap,aw], Y.Q. Wang [y], Z. Wang [a,ap], Z.G. Wang [a,ap], Z.H. Wang [bc,ap], Z.Y. Wang [a], Zongyuan Wang [a,aw], T. Weber [y], D.H. Wei [k], P. Weidenkaff [y], S.P. Wen [a], U. Wiedner [d], M. Wolke [bi], L.H. Wu [a], L.J. Wu [a,aw], Z. Wu [a,ap], L. Xia [bc,ap], X. Xia [aj], Y. Xia [r], D. Xiao [a], H. Xiao [bd], Y.J. Xiao [a,aw], Z.J. Xiao [ae], Y.G. Xie [a,ap], Y.H. Xie [f], X.A. Xiong [a,aw], Q.L. Xiu [a,ap], G.F. Xu [a], J.J. Xu [a,aw], L. Xu [a], Q.J. Xu [m], Q.N. Xu [aw], X.P. Xu [an], L. Yan [bf,bh], W.B. Yan [bc,ap], W.C. Yan [bc,ap], W.C. Yan [b], Y.H. Yan [r], H.J. Yang [ak,8], H.X. Yang [a], L. Yang [bj], Y.H. Yang [af], Y.X. Yang [k], Yifan Yang [a,aw], M. Ye [a,ap], M.H. Ye [g], J.H. Yin [a], Z.Y. You [aq], B.X. Yu [a,ap,aw], C.X. Yu [ag], J.S. Yu [ac], C.Z. Yuan [a,aw], Y. Yuan [a], A. Yuncu [at,1], A.A. Zafar [be], A. Zallo [t], Y. Zeng [r], Z. Zeng [bc,ap], B.X. Zhang [a], B.Y. Zhang [a,ap], C.C. Zhang [a], D.H. Zhang [a], H.H. Zhang [aq], H.Y. Zhang [a,ap], J. Zhang [a,aw], J.L. Zhang [a], J.Q. Zhang [a], J.W. Zhang [a,ap,aw], J.Y. Zhang [a], J.Z. Zhang [a,aw], K. Zhang [a,aw], L. Zhang [ar], S.Q. Zhang [ag], X.Y. Zhang [aj], Y.H. Zhang [a,ap], Y.T. Zhang [bc,ap], Yang Zhang [a], Yao Zhang [a], Yu Zhang [aw], Z.H. Zhang [f], Z.P. Zhang [bc], Z.Y. Zhang [bj], G. Zhao [a], J.W. Zhao [a,ap], J.Y. Zhao [a,aw], J.Z. Zhao [a,ap], Lei Zhao [bc,ap], Ling Zhao [a], M.G. Zhao [ag], Q. Zhao [a], S.J. Zhao [bl], T.C. Zhao [a], Y.B. Zhao [a,ap], Z.G. Zhao [bc,ap], A. Zhemchugov [z,2], B. Zheng [bd], J.P. Zheng [a,ap], W.J. Zheng [aj], Y.H. Zheng [aw], B. Zhong [ae], L. Zhou [a,ap], X. Zhou [bj], X.K. Zhou [bc,ap], X.R. Zhou [bc,ap], X.Y. Zhou [a], Y.X. Zhou [l], J. Zhu [ag], J. Zhu [aq], K. Zhu [a], K.J. Zhu [a,ap,aw], S. Zhu [a], S.H. Zhu [bb], X.L. Zhu [ar], Y.C. Zhu [bc,ap], Y.S. Zhu [a,aw], Z.A. Zhu [a,aw], J. Zhuang [a,ap], B.S. Zou [a], J.H. Zou [a]

[a] *Institute of High Energy Physics, Beijing 100049, People's Republic of China*
[b] *Beihang University, Beijing 100191, People's Republic of China*
[c] *Beijing Institute of Petrochemical Technology, Beijing 102617, People's Republic of China*
[d] *Bochum Ruhr-University, D-44780 Bochum, Germany*
[e] *Carnegie Mellon University, Pittsburgh, PA 15213, USA*
[f] *Central China Normal University, Wuhan 430079, People's Republic of China*
[g] *China Center of Advanced Science and Technology, Beijing 100190, People's Republic of China*
[h] *COMSATS Institute of Information Technology, Lahore, Defence Road, Off Raiwind Road, 54000 Lahore, Pakistan*
[i] *G.I. Budker Institute of Nuclear Physics SB RAS (BINP), Novosibirsk 630090, Russia*
[j] *GSI Helmholtzcentre for Heavy Ion Research GmbH, D-64291 Darmstadt, Germany*
[k] *Guangxi Normal University, Guilin 541004, People's Republic of China*
[l] *Guangxi University, Nanning 530004, People's Republic of China*
[m] *Hangzhou Normal University, Hangzhou 310036, People's Republic of China*
[n] *Helmholtz Institute Mainz, Johann-Joachim-Becher-Weg 45, D-55099 Mainz, Germany*
[o] *Henan Normal University, Xinxiang 453007, People's Republic of China*
[p] *Henan University of Science and Technology, Luoyang 471003, People's Republic of China*
[q] *Huangshan College, Huangshan 245000, People's Republic of China*
[r] *Hunan University, Changsha 410082, People's Republic of China*
[s] *Indiana University, Bloomington, IN 47405, USA*
[t] *INFN Laboratori Nazionali di Frascati, I-00044, Frascati, Italy*
[u] *INFN and University of Perugia, I-06100, Perugia, Italy*
[v] *INFN Sezione di Ferrara, I-44122, Ferrara, Italy*
[w] *University of Ferrara, I-44122, Ferrara, Italy*
[x] *Institute of Physics and Technology, Peace Ave. 54B, Ulaanbaatar 13330, Mongolia*
[y] *Johannes Gutenberg University of Mainz, Johann-Joachim-Becher-Weg 45, D-55099 Mainz, Germany*
[z] *Joint Institute for Nuclear Research, 141980 Dubna, Moscow region, Russia*
[aa] *Justus-Liebig-Universitaet Giessen, II. Physikalisches Institut, Heinrich-Buff-Ring 16, D-35392 Giessen, Germany*
[ab] *KVI-CART, University of Groningen, NL-9747 AA Groningen, the Netherlands*
[ac] *Lanzhou University, Lanzhou 730000, People's Republic of China*
[ad] *Liaoning University, Shenyang 110036, People's Republic of China*
[ae] *Nanjing Normal University, Nanjing 210023, People's Republic of China*
[af] *Nanjing University, Nanjing 210093, People's Republic of China*
[ag] *Nankai University, Tianjin 300071, People's Republic of China*
[ah] *Peking University, Beijing 100871, People's Republic of China*

[ai] Seoul National University, Seoul, 151-747, Republic of Korea
[aj] Shandong University, Jinan 250100, People's Republic of China
[ak] Shanghai Jiao Tong University, Shanghai 200240, People's Republic of China
[al] Shanxi University, Taiyuan 030006, People's Republic of China
[am] Sichuan University, Chengdu 610064, People's Republic of China
[an] Soochow University, Suzhou 215006, People's Republic of China
[ao] Southeast University, Nanjing 211100, People's Republic of China
[ap] State Key Laboratory of Particle Detection and Electronics, Beijing 100049, Hefei 230026, People's Republic of China
[aq] Sun Yat-Sen University, Guangzhou 510275, People's Republic of China
[ar] Tsinghua University, Beijing 100084, People's Republic of China
[as] Ankara University, 06100 Tandogan, Ankara, Turkey
[at] Istanbul Bilgi University, 34060 Eyup, Istanbul, Turkey
[au] Uludag University, 16059 Bursa, Turkey
[av] Near East University, Nicosia, North Cyprus, Mersin 10, Turkey
[aw] University of Chinese Academy of Sciences, Beijing 100049, People's Republic of China
[ax] University of Hawaii, Honolulu, HI 96822, USA
[ay] University of Jinan, Jinan 250022, People's Republic of China
[az] University of Minnesota, Minneapolis, MN 55455, USA
[ba] University of Muenster, Wilhelm-Klemm-Str. 9, 48149 Muenster, Germany
[bb] University of Science and Technology Liaoning, Anshan 114051, People's Republic of China
[bc] University of Science and Technology of China, Hefei 230026, People's Republic of China
[bd] University of South China, Hengyang 421001, People's Republic of China
[be] University of the Punjab, Lahore-54590, Pakistan
[bf] University of Turin, I-10125, Turin, Italy
[bg] University of Eastern Piedmont, I-15121, Alessandria, Italy
[bh] INFN, I-10125, Turin, Italy
[bi] Uppsala University, Box 516, SE-75120 Uppsala, Sweden
[bj] Wuhan University, Wuhan 430072, People's Republic of China
[bk] Zhejiang University, Hangzhou 310027, People's Republic of China
[bl] Zhengzhou University, Zhengzhou 450001, People's Republic of China

ARTICLE INFO

Article history:
Received 3 August 2018
Received in revised form 22 February 2019
Accepted 3 March 2019
Available online 6 March 2019
Editor: M. Doser

Keywords:
Phase
Strong amplitude
Electromagnetic amplitude
J/ψ decay
BESIII

ABSTRACT

Using 16 energy points of e^+e^- annihilation data collected in the vicinity of the J/ψ resonance with the BESIII detector and with a total integrated luminosity of around 100 pb^{-1}, we study the relative phase between the strong and electromagnetic amplitudes of J/ψ decays. The relative phase between J/ψ electromagnetic decay and the continuum process (e^+e^- annihilation without the J/ψ resonance) is confirmed to be zero by studying the cross section lineshape of $\mu^+\mu^-$ production. The relative phase between J/ψ strong and electromagnetic decays is then measured to be $(84.9 \pm 3.6)^\circ$ or $(-84.7 \pm 3.1)^\circ$ for the $2(\pi^+\pi^-)\pi^0$ final state by investigating the interference pattern between the J/ψ decay and the continuum process. This is the first measurement of the relative phase between J/ψ strong and electromagnetic decays into a multihadron final state using the lineshape of the production cross section. We also study the production lineshape of the multihadron final state $\eta\pi^+\pi^-$ with $\eta \to \pi^+\pi^-\pi^0$, which provides additional information about the phase between the J/ψ electromagnetic decay amplitude and the continuum process. Additionally, the branching fraction of $J/\psi \to 2(\pi^+\pi^-)\pi^0$ is measured to be $(4.73 \pm 0.44)\%$ or $(4.85 \pm 0.45)\%$, and the branching fraction of $J/\psi \to \eta\pi^+\pi^-$ is measured to be $(3.78 \pm 0.68) \times 10^{-4}$. Both of them are consistent with the world average values. The quoted uncertainties include both statistical and systematic uncertainties, which are mainly caused by the low statistics.

1. Introduction

The relative phase between the strong and electromagnetic (EM) amplitudes of quarkonium decays is a basic parameter that provides insight into the dynamics of quarkonium decays. As shown in Fig. 1, in the vicinity of the J/ψ, the annihilation of e^+e^- into a hadronic final state proceeds through three processes: strong decay of the J/ψ (mediated by gluons), EM decay of the J/ψ (mediated by a virtual photon), and the continuum process (without a J/ψ intermediate state and mediated by a virtual photon). For leptonic final states, on the other hand, the strong decay is absent. In perturbative quantum chromodynamics, the relative phase ($\Phi_{g,\gamma}$) between the charmonium strong decay amplitude (A_g) and the EM amplitude (A_γ) is predicted to be 0° or 180° [1,2] at lowest order.

In contrast to this prediction, model-dependent analyses using SU(3) flavor symmetry suggest that $\Phi_{g,\gamma}$ is 90° for J/ψ two-body

* Corresponding author.
E-mail address: yadiwang@uni-mainz.de (Y.D. Wang).

[1] Also at Bogazici University, 34342 Istanbul, Turkey.
[2] Also at the Moscow Institute of Physics and Technology, Moscow 141700, Russia.
[3] Also at the Functional Electronics Laboratory, Tomsk State University, Tomsk, 634050, Russia.
[4] Also at the Novosibirsk State University, Novosibirsk, 630090, Russia.
[5] Also at the NRC "Kurchatov Institute", PNPI, 188300, Gatchina, Russia.
[6] Also at Istanbul Arel University, 34295 Istanbul, Turkey.
[7] Also at Goethe University Frankfurt, 60323 Frankfurt am Main, Germany.
[8] Also at Key Laboratory for Particle Physics, Astrophysics and Cosmology, Ministry of Education; Shanghai Key Laboratory for Particle Physics and Cosmology; Institute of Nuclear and Particle Physics, Shanghai 200240, People's Republic of China.
[9] Government College Women University, Sialkot - 51310, Punjab, Pakistan.
[10] Currently at: Center for Underground Physics, Institute for Basic Science, Daejeon 34126, Korea.

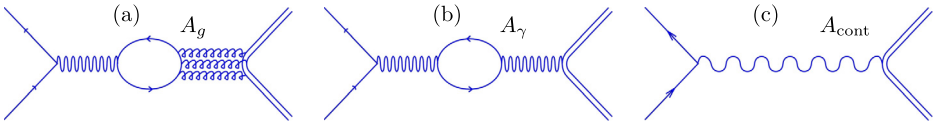

Fig. 1. The Feynman diagrams for the process $e^+e^-\to$ hadrons: (a) J/ψ strong decay *via* gluons, (b) J/ψ EM decay *via* one virtual photon, (c) the continuum decay *via* a virtual photon.

decays into meson pairs with quantum numbers ($J^{\rm P}$) of 1^-0^- [3,4], 0^-0^- [5–7], 1^-1^- [7], and 1^+0^- [8], and for J/ψ decays into $N\bar{N}$ baryon pairs [9,10]. Similar analyses suggest $\psi(2S)$ decays to pairs of pseudoscalar mesons also have a phase $\Phi_{g,\gamma}$ around 90°, but $\psi(2S)$ decays to pairs of mesons with 1^-0^- and 1^+0^- have a different value of $\Phi_{g,\gamma}$ [8,11].

Several theoretical ideas regarding the origin and implications of $\Phi_{g,\gamma}$ have been proposed. Based on unsubtracted dispersion relations and asymptotic freedom, the Okubo-Zweig-Iizuka-rule-violating amplitude with respect to the virtual photon contribution is predominately imaginary [12]. An orthogonal phase in J/ψ decays is also expected if any vector quarkonium is assumed to be coupled to a vector glueball [13–15]. Furthermore, it has been advocated [8,15] that different phases for the J/ψ and $\psi(2S)$ decay, namely $\sim 90°$ and $\sim 180°$, respectively, can explain the long-standing $\rho\pi$ puzzle of charmonium physics. However, there is no simple explanation that the phase should be 90°.

An independent approach for measuring the relative phases of the diagrams in Fig. 1 consists of extracting the interference pattern of the e^+e^- reaction cross section as a function of the center-of-mass (CM) energy (W) in the vicinity of a resonance. The Born cross section of a pure EM process can be written as

$$\sigma^0(W)\propto|A_\gamma(W)e^{i\Phi_{\gamma,\rm cont}}+A_{\rm cont}(W)|^2.$$

The relative phase ($\Phi_{\gamma,\rm cont}$) between the J/ψ EM amplitude (A_γ) and the continuum amplitude ($A_{\rm cont}$) has previously been assumed to be zero degrees and this assumption has been shown to be consistent with the observed interference pattern in J/ψ decays to lepton pairs [16–19]. The full cross section for processes including the strong and EM amplitudes can be written as

$$\sigma^0(W)\propto|[A_g(W)e^{i\Phi_{g,\gamma}}+A_\gamma(W)]e^{i\Phi_{\gamma,\rm cont}}+A_{\rm cont}(W)|^2.$$

If we take the phase $\Phi_{\gamma,\rm cont}$ to be zero, as measurements suggest, the Born cross section is simplified to be:

$$\sigma^0(W)\propto|A_g(W)e^{i\Phi_{g,\rm EM}}+A_\gamma(W)+A_{\rm cont}(W)|^2,$$

where $\Phi_{g,\rm EM}$ is the phase between the strong and the full EM amplitudes.

It is argued that the relative phases $\Phi_{\gamma,\rm cont}$ and $\Phi_{g,\rm EM}$ are universal in all exclusive decay modes [20]. In this Letter, we first analyze the process $e^+e^-\to\mu^+\mu^-$ and confirm the phase $\Phi_{\gamma,\rm cont}$ is consistent with zero. We also use this process to extract the CM energy spread and the overall energy scale, which are essential accelerator parameters that are used as input for the other analyses. Then, we measure the phase $\Phi_{g,\rm EM}$ by analyzing the process $e^+e^-\to 2(\pi^+\pi^-)\pi^0$ (abbreviated as 5π). We chose this process because it both has a large branching fraction in J/ψ decays and has a sizable cross section of the continuum decay. We also study the process $e^+e^-\to\eta\pi^+\pi^-$ with η decaying into $\pi^+\pi^-\pi^0$. Since it proceeds largely through $\eta\rho^0$, which is an EM process due to G-parity conservation, this process is used to gain further information about $\Phi_{\gamma,\rm cont}$. This is the first measurement of the phases $\Phi_{g,\rm EM}$ and $\Phi_{\gamma,\rm cont}$ in the interference pattern of the cross section lineshape in the vicinity of the J/ψ and the first time using multihadron final states.

Table 1
The CM energy (W_i) and the integrated luminosity ($\mathcal{L}_i$) for each data point. The uncertainty of W_i is from the BEMS measurement, and the uncertainty of $\mathcal{L}_i$ is the statistical and systematic uncertainties added in quadrature [22].

No.	W_i (MeV)	$\mathcal{L}_i$ (pb^{-1})
1	3050.21 ± 0.03	14.92 ± 0.16
2	3059.26 ± 0.03	15.06 ± 0.16
3	3080.20 ± 0.02	17.39 ± 0.19
4	3083.06 ± 0.04	4.77 ± 0.06
5	3089.42 ± 0.02	15.56 ± 0.17
6	3092.32 ± 0.03	14.91 ± 0.16
7	3095.26 ± 0.08	2.14 ± 0.03
8	3095.99 ± 0.08	1.82 ± 0.02
9	3096.39 ± 0.08	2.14 ± 0.03
10	3097.78 ± 0.08	2.07 ± 0.03
11	3098.90 ± 0.08	2.20 ± 0.03
12	3099.61 ± 0.09	0.76 ± 0.01
13	3101.92 ± 0.11	1.61 ± 0.02
14	3106.14 ± 0.09	2.11 ± 0.03
15	3112.62 ± 0.09	1.72 ± 0.02
16	3120.44 ± 0.12	1.26 ± 0.02

This letter is organized as follows: in Section 2, the BESIII detector and the data sets being used are described. In Section 3, the event selection, the efficiency, the observed cross section and the systematic uncertainties of $e^+e^-\to\mu^+\mu^-$, 5π and $\eta\pi^+\pi^-$ are described. In Section 4, the fit to the cross section lineshapes of $e^+e^-\to\mu^+\mu^-$, 5π and $\eta\pi^+\pi^-$ as well as the results are reported. The results are summarized in Section 5.

2. BESIII experiment and data sets

The BEPCII is a double-ring e^+e^- collider running at CM energies between $2.0-4.6$ GeV and it has reached its design luminosity of 1.0×10^{33} cm^{-2}s^{-1} at a CM energy of 3770 MeV. The cylindrical BESIII detector has an effective geometrical acceptance of 93% of 4π solid angle and it is divided into a barrel section and two endcaps. It consists of a small-cell, helium-based multilayer drift chamber (MDC), a plastic scintillator time-of-flight system (TOF), a CsI(Tl) (Thallium doped Cesium Iodide) crystal electromagnetic calorimeter (EMC) and a muon system containing resistive plate chambers in the iron return yoke of a 1 Tesla (0.9 Tesla for data sets used in this letter) superconducting solenoid. The momentum resolution for charged tracks is 0.5% for 1 GeV/c momentum tracks. The time resolution in the barrel (endcaps) is 80 ps (110 ps). The photon energy resolution at 1 GeV is 2.5% (5%) in the barrel (endcaps) of the EMC. Further details about the BESIII detector are described in Ref. [21].

This analysis uses data samples collected in 2012 at 16 different CM energies with a total integrated luminosity of about 100 pb^{-1} [22]. The CM energies, W_i, and the integrated luminosities, $\mathcal{L}_i$, of each data sample are summarized in Table 1. The CM energies are measured by the Beam Energy Measurement System (BEMS), in which photons from a CO_2 laser are Compton backscattered off the electron beam and detected by a high-purity Germanium detector [23]. The integrated luminosities are determined using two-gamma events [22].

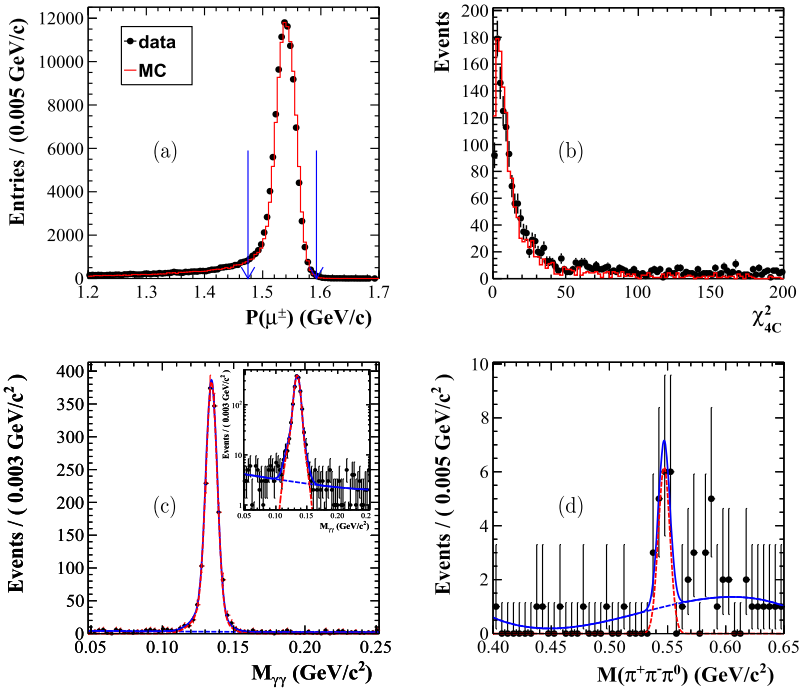

Fig. 2. (a) Comparison between data and BABAYAGA MC sample for the momentum of the $\mu^{\pm}$ for $e^+e^- \to \mu^+\mu^-$ candidate events. The region between the arrows denotes the signal window. (b) Comparison between data and MC simulation for the χ^2_{4C} in the $e^+e^- \to 5\pi$ channel. (c) The fit of the $M_{\gamma\gamma}$ spectrum, and the inset is in the logarithmic scale. (d) The fit of the $M^{\eta}_{\pi^+\pi^-\gamma\gamma}$ spectrum. All plots are taken at $W = 3092.32$ MeV, and the black dots with error bars are for data. For (a) and (b), the red histograms denote the MC samples. For (c) and (d), the red dashed lines denote the signal, the blue dotted lines are for the background, the blue solid lines represent the overall fit curve.

A GEANT4-based [24] simulation software package including a description of the geometry and material and the detector response is used to generate Monte Carlo (MC) samples. The BABAYAGA [25] generator which includes interference between $A_{\rm cont}$ and A_γ is used to simulate the $e^+e^- \to \mu^+\mu^-$ and the $e^+e^- \to e^+e^-$ events. The samples $e^+e^- \to 5\pi$ and intermediate processes $e^+e^- \to \rho^0\rho^{\pm}\pi^{\mp}$, $e^+e^- \to \rho^0 f_2(1275)\pi^0$, $e^+e^- \to \omega\pi^+\pi^-$ and $e^+e^- \to \eta\pi^+\pi^-$ are generated assuming a uniform phase space distribution. The intermediate decays $e^+e^- \to \eta\rho^0$ and $\eta\omega$ and the subsequent decay of all intermediate states are generated with EVTGEN [26,27]. For the 5π system, the polar angular distributions for each of the pions in the e^+e^- CM frame are tuned to be the same as those in data. The MCGPJ [28] generator is used to incorporate radiation effects in the $e^+e^- \to 5\pi$ process. The possible interference between A_g and $A_{\rm cont}$ (or A_γ) is included in the MCGPJ generator. The output cross section from the MCGPJ generator is tuned to be the same as the observed cross section of $e^+e^- \to 5\pi$. A MC sample of J/ψ inclusive decays is used to explore possible hadronic background. In this sample, the known decay modes are generated with EVTGEN incorporating the branching fractions from the Particle Data Group (PDG) [29] and the remaining unknown decays are generated according to the LUNDCHARM [30] model. The CM energy spread is incorporated in all MC samples.

3. Analysis

3.1. Event selection for the $e^+e^- \to \mu^+\mu^-$ process

Events of $e^+e^- \to \mu^+\mu^-$ are required to have only two charged tracks with opposite charge. The charged tracks are required to originate from the interaction region which is defined as a cylinder with a radius of 1 cm and an axial distance from the interaction point of ± 10 cm. The polar angle θ of each track with respect to the positron beam is required to be within the barrel region ($|\cos\theta| < 0.8$). Each charged track must have hit information in the EMC, and its measured energy deposit divided by its momentum obtained from the MDC (E/p) is required to be less than 0.3 to suppress $e^+e^- \to e^+e^-$ and hadronic final state events. Cosmic rays are rejected by requiring $\Delta T \equiv |T_{\rm trk1} - T_{\rm trk2}| < 4$ ns, where $T_{\rm trk1}$ and $T_{\rm trk2}$ are the measured flight times in the TOF detector for the two tracks. The improved track parameters obtained from the vertex fit, which constrains the two tracks to a common vertex, are used in further analysis. The momenta of muon candidates must satisfy $(p_{\rm the} - 4\sigma_p) < p_{\mu^{\pm}} < (p_{\rm the} + 3\sigma_p)$, where $p_{\rm the}$ and σ_p are the nominal value and experimental resolution of the momentum of $\mu^{\pm}$, respectively. Fig. 2 (a) shows the momentum distributions of data and the BABAYAGA MC sample at $W = 3092.32$ MeV. Throughout this letter, all the performance plots are from the same energy point. The data appear to be consistent with the MC simulations.

Potential two-body decay backgrounds are estimated by investigating the exclusive MC samples of $e^+e^- \to p\bar{p}$, K^+K^-, $\pi^+\pi^-$, and e^+e^-. Only the process $e^+e^- \to \pi^+\pi^-$ is found to be a potential background. According to Ref. [31], the cross section of $\pi^+\pi^-$ is about 10^{-2} nb at 3000 MeV, which is negligible compared to that of $\mu^+\mu^-$ of about 10 nb. At the J/ψ peak, the ratio between the branching fraction of $J/\psi \to \pi^+\pi^-$ and that of $J/\psi \to \mu^+\mu^-$ is about 0.2%. Taking into account the selection efficiency, where that of $e^+e^- \to \pi^+\pi^-$ is about one third of that of $e^+e^- \to \mu^+\mu^-$, the background from the $\pi^+\pi^-$ final state can safely be ignored. From a study of the J/ψ inclusive MC sample, the contribution from the remaining multihadron events is about 0.2% of the surviving events and is also negligible.

3.2. Event selection for the $e^+e^- \to 5\pi$ and $\eta\pi^+\pi^-$ processes

The events are required to have four charged tracks with a net charge of zero and at least two photons. The charged tracks are re-

quired to originate from the interaction region, while their polar angles are required to be within a range of $|\cos\theta| < 0.93$. Charged particle identification is performed by combining the ionization energy loss (dE/dx) in the MDC and the flight times in the TOF. For each track, the probability for the pion particle hypothesis is required to be larger than that for the kaon particle hypothesis. The photons are required to have a deposited energy greater than 50 MeV in the endcap ($0.86 < |\cos\theta| < 0.92$) or 25 MeV in the barrel ($|\cos\theta| < 0.8$) of the EMC. To suppress electronic noise and energy deposits unrelated to the event, the time of the cluster signal given by the EMC must be within 700 ns after the reconstructed event start time. To exclude clusters originating from charged tracks, the angle between the photon candidate and the nearest charged track is required to be greater than 10°.

After constraining the four charged tracks to a common vertex using a vertex fit, a four-constraint (4C) kinematic fit imposing energy and momentum conservation is performed to the $e^+e^- \to 2(\pi^+\pi^-)\gamma\gamma$ hypothesis. Events with $\chi^2_{\rm 4C} < 200$ are retained, and at least 80% of the background is rejected and about 95% signal is retained. If there are more than two photons, all combinations of photon pairs are tried and that with the least $\chi^2_{\rm 4C}$ value is retained. Fig. 2 (b) shows the distribution of $\chi^2_{\rm 4C}$ for the data and MC simulation. The invariant mass of the photon pair $M_{\gamma\gamma}$ is required to be within the range $(0.0, 0.3)$ GeV/c^2. The decay angle ($\theta_{\rm decay}$) of a photon is defined as the polar angle measured in the π^0 rest frame with respect to the π^0 direction in the e^+e^- CM frame. The cosine of the decay angle ($\cos\theta_{\rm decay}$) is required to be lower than 0.9 to remove wrong photon combinations.

By studying the inclusive and exclusive MC samples, the backgrounds can be classified into $e^+e^- \to \gamma 2(\pi^+\pi^-)$, $\gamma 2(\pi^+\pi^-)\pi^0$ and $2(\pi^+\pi^-\pi^0)$ (abbreviated as $\gamma 4\pi$, $\gamma 5\pi$, and 6π) according to the number of photons in the final states. For normalization, the background channels are normalized according to their branching fractions from J/ψ [29] decay or their energy-dependent cross section measured by BaBar [32]. Only the $e^+e^- \to \gamma 5\pi$ makes a peaking background of less than 1% of the π^0 events on the spectrum of $M_{\gamma\gamma}$.

The surviving candidate events include events from the process with an η intermediate state, i.e. $e^+e^- \to \eta\pi^+\pi^-$ with η decays to $\pi^+\pi^-\pi^0$. Due to G-parity conservation, the dominant process $e^+e^- \to \eta\rho^0 \to \eta\pi^+\pi^-$ is allowed only via EM decay, and will affect the measurement of $\Phi_{g,\rm EM}$ for the process $e^+e^- \to 5\pi$. Thus, the process of $e^+e^- \to \eta\pi^+\pi^-$ will be separated from the inclusive $e^+e^- \to 5\pi$, and measured alone. In the inclusive $e^+e^- \to 5\pi$ candidate events, we reconstructed the η signal with the $\pi^+\pi^-\gamma\gamma$ combination whose invariant mass $M^{\eta}_{\pi^+\pi^-\gamma\gamma}$ is closest to the η nominal mass. The signal candidate of $e^+e^- \to 5\pi$ is then selected by imposing a further requirement of $M^{\eta}_{\pi^+\pi^-\gamma\gamma} < 0.517$ MeV/c^2 or $M^{\eta}_{\pi^+\pi^-\gamma\gamma} > 0.577$ MeV/c^2. The corresponding yield is determined by fitting the distribution of $\gamma\gamma$ invariant mass, $M_{\gamma\gamma}$, with a double Gaussian function for the signal and a second-order polynomial function for background, as shown in Fig. 2 (c). The yield of $e^+e^- \to \eta\pi^+\pi^-$ is determined by fitting the $M^{\eta}_{\pi^+\pi^-\gamma\gamma}$ distribution, where the η signal is modeled by a Gaussian function and the background is described by a third- or lower-order polynomial function, as presented in Fig. 2 (d). To better describe the data, the parameters of the η and π^0 signal lineshapes are fixed to values obtained from fits to distributions summed over all CM energies.

3.3. Cross sections of $e^+e^- \to \mu^+\mu^-$, 5π and $\eta\pi^+\pi^-$

The observed cross section is calculated with

$$\sigma_i^{\rm obs} = \frac{N_i}{\epsilon_i \times \mathcal{L}_i(\times\mathcal{B})},$$

where N_i is the number of observed signal events, ϵ_i is the efficiency given by the MC simulations, and $\mathcal{L}_i$ is the luminosity listed in Table 1. In the equation, $\mathcal{B}$ denotes the branching fractions of intermediate decays, and is $\mathcal{B}(\pi^0 \to \gamma\gamma)$ for $e^+e^- \to 5\pi$ and $\mathcal{B}(\eta \to \pi^+\pi^-\pi^0) \times \mathcal{B}(\pi^0 \to \gamma\gamma)$ for $e^+e^- \to \eta\pi^+\pi^-$. For $e^+e^- \to \mu^+\mu^-$, the efficiency from the BABAYAGA simulation includes the radiative effects [25].

For the process $e^+e^- \to 5\pi$, to take into account kinematic effects of the intermediate states, the weighted-average efficiency $\epsilon_i^{\rm com}$ obtained according to the relative production rates between the processes with different intermediate states is used. The interference among different intermediate processes is assumed to be independent of the phase measurement and not taken into account. To take into account the radiation effect, an additional CM energy-dependent correction factor, $f_i^{\rm EC}$ is used, which is the ratio of the detection efficiencies of $e^+e^- \to 5\pi$ at the i-th CM energy point estimated with the generator MCGPJ to that at the J/ψ peak. The generator MCGPJ models radiation effect for the process $e^+e^- \to 5\pi$ properly by adjusting the output cross section to be the same as the calculated $\sigma_i^{\rm obs}$ from data. Thus, the effective detection efficiency is $\epsilon_i = f_i^{\rm EC} \times \epsilon_i^{\rm com}$.

From the PDG, we know the decays $J/\psi \to \eta\rho$, $\eta\omega$, and $\eta\pi^+\pi^-$ also exist, even though the measured branching ratios are very old and have large uncertainties. According to MC simulations, the efficiencies for these processes are nearly the same. Thus, the efficiency of the MC sample for $e^+e^- \to \eta\pi^+\pi^-$, without intermediate states, is used in the cross section calculation. The efficiency correction factor $f_i^{\rm EC}$ is not implemented due to the large statistical uncertainty of its cross section and the small effect of $f_i^{\rm EC}$ on the phase measurement (see the results of the 5π in Section 4). The calculated cross sections for $e^+e^- \to \mu^+\mu^-$, 5π and $\eta\pi^+\pi^-$, together with the efficiencies and the number of events, are listed in Table 2.

3.4. Systematic uncertainties

Systematic uncertainties are divided into two categories. Those that are universal among the different energy points include those related to the event selection efficiencies, intermediate states in $e^+e^- \to \eta\pi^+\pi^-$, and the branching fractions of intermediate state decays. Those that are not universal are treated separately for all energy points, which include the uncertainties related to the fits to the spectra, $\epsilon_i^{\rm com}$ of $e^+e^- \to 5\pi$, and the luminosities.

The systematic uncertainty of the tracking of muons is studied with a control sample of $J/\psi \to \mu^+\mu^-$ selected with more stringent criteria on one tagged charged track. The efficiency is the rate to detect another charged track on the recoil side of the tagged track. The difference on the efficiency is 1% between data and MC simulation, which is treated as the systematic uncertainty. The systematic uncertainties associated with the tracking and the particle identification for pion candidates are investigated using a control sample of $J/\psi \to p\bar{p}\pi^+\pi^-$, and are found to be 1% individually [33]. Dedicated studies on $e^+e^- \to \gamma\mu^+\mu^-$ [34] and $J/\psi \to \pi^+\pi^-\pi^0$ [35] conclude that the systematic uncertainty due to photon identification is 1% per photon. The systematic uncertainty related to the 4C kinematic fit is determined by changing the $\chi^2_{\rm 4C}$ requirement, and found to be 1%. The uncertainties of the branching fractions for the intermediate-state decays $\pi^0 \to \gamma\gamma$

Table 2
The number of events, efficiency and the observed cross section for $e^+e^- \to \mu^+\mu^-$, 5π and $\eta\pi^+\pi^-$ at each energy point. Statistical uncertainties are quoted for the number of events and the efficiencies, while both statistical and systematic uncertainties are quoted for the cross section.

No.	$\mu^+\mu^-$			5π		
	N_i	ϵ_i (%)	$\sigma_i^{\rm obs}$ (nb)	N_i	ϵ_i (%)	$\sigma_i^{\rm obs}$ (nb)
1	76553 ± 277	54.52 ± 0.16	$9.411 \pm 0.034 \pm 0.217$	734 ± 29	23.60 ± 1.28	$0.211 \pm 0.008 \pm 0.017$
2	76058 ± 276	54.53 ± 0.16	$9.261 \pm 0.034 \pm 0.213$	723 ± 28	23.88 ± 1.43	$0.204 \pm 0.008 \pm 0.017$
3	81532 ± 286	53.30 ± 0.16	$8.794 \pm 0.031 \pm 0.202$	765 ± 29	23.54 ± 1.25	$0.189 \pm 0.007 \pm 0.015$
4	21584 ± 147	53.74 ± 0.16	$8.42 \pm 0.06 \pm 0.20$	180 ± 14	24.31 ± 3.02	$0.158 \pm 0.012 \pm 0.021$
5	63674 ± 252	52.76 ± 0.16	$7.758 \pm 0.031 \pm 0.177$	858 ± 30	25.16 ± 1.27	$0.222 \pm 0.008 \pm 0.017$
6	51677 ± 227	51.12 ± 0.16	$6.780 \pm 0.030 \pm 0.155$	1434 ± 39	26.09 ± 1.02	$0.373 \pm 0.010 \pm 0.027$
7	15929 ± 126	58.84 ± 0.16	$12.63 \pm 0.10 \pm 0.30$	4962 ± 71	28.69 ± 0.60	$8.16 \pm 0.12 \pm 0.53$
8	52001 ± 228	63.23 ± 0.17	$45.28 \pm 0.20 \pm 1.07$	18120 ± 140	28.37 ± 0.40	$35.59 \pm 0.27 \pm 2.26$
9	154741 ± 393	63.87 ± 0.15	$113.47 \pm 0.29 \pm 2.67$	52380 ± 230	28.42 ± 0.35	$87.4 \pm 0.4 \pm 5.5$
10	281713 ± 531	63.99 ± 0.16	$212.8 \pm 0.4 \pm 5.1$	90560 ± 310	28.19 ± 0.31	$157.1 \pm 0.5 \pm 9.9$
11	155118 ± 394	64.07 ± 0.16	$109.90 \pm 0.28 \pm 2.60$	43520 ± 210	28.32 ± 0.36	$70.57 \pm 0.34 \pm 4.47$
12	26646 ± 163	62.62 ± 0.15	$56.29 \pm 0.35 \pm 1.39$	6424 ± 81	28.41 ± 0.52	$30.3 \pm 0.4 \pm 2.0$
13	21893 ± 148	60.51 ± 0.15	$22.44 \pm 0.15 \pm 0.54$	3440 ± 60	26.57 ± 0.68	$8.13 \pm 0.14 \pm 0.54$
14	20184 ± 142	58.74 ± 0.16	$16.32 \pm 0.12 \pm 0.38$	2468 ± 50	27.89 ± 0.79	$4.25 \pm 0.09 \pm 0.29$
15	13173 ± 115	57.72 ± 0.16	$13.27 \pm 0.12 \pm 0.32$	1160 ± 35	26.72 ± 1.11	$2.55 \pm 0.08 \pm 0.19$
16	8550 ± 93	56.40 ± 0.16	$11.99 \pm 0.13 \pm 0.29$	623 ± 26	26.63 ± 1.43	$1.87 \pm 0.08 \pm 0.15$

No.	$\eta\pi^+\pi^-$		
	N_i	ϵ_i (%)	$\sigma_i^{\rm obs}$ (nb)
1	32 ± 6	21.16 ± 0.11	$0.045 \pm 0.009 \pm 0.006$
2	24 ± 6	21.08 ± 0.11	$0.034 \pm 0.008 \pm 0.004$
3	34 ± 6	20.78 ± 0.10	$0.042 \pm 0.008 \pm 0.006$
4	8 ± 3	21.07 ± 0.11	$0.037 \pm 0.015 \pm 0.005$
5	25 ± 6	21.11 ± 0.11	$0.033 \pm 0.007 \pm 0.004$
6	15 ± 5	21.14 ± 0.11	$0.0216 \pm 0.0064 \pm 0.0025$
7	10 ± 4	21.25 ± 0.11	$0.100 \pm 0.039 \pm 0.013$
8	19 ± 7	20.94 ± 0.11	$0.218 \pm 0.076 \pm 0.027$
9	60 ± 11	21.00 ± 0.11	$0.59 \pm 0.11 \pm 0.07$
10	118 ± 15	20.79 ± 0.10	$1.21 \pm 0.15 \pm 0.15$
11	74 ± 11	20.83 ± 0.10	$0.709 \pm 0.105 \pm 0.088$
12	22 ± 6	20.50 ± 0.10	$0.63 \pm 0.16 \pm 0.08$
13	12 ± 4	20.84 ± 0.10	$0.155 \pm 0.056 \pm 0.020$
14	7 ± 3	20.71 ± 0.10	$0.072 \pm 0.034 \pm 0.009$
15	5 ± 3	20.58 ± 0.10	$0.057 \pm 0.036 \pm 0.007$
16	6 ± 3	20.63 ± 0.10	$0.094 \pm 0.045 \pm 0.012$

and $\eta \to \pi^+\pi^-\pi^0$ from the PDG [29] are considered in the systematic uncertainty.

The requirements of $\cos\theta$, E/p, $|\Delta T|$ and $p_{\mu^\pm}$ in the selection of $e^+e^- \to \mu^+\mu^-$, and $M^{\eta}_{\pi^+\pi^-\gamma\gamma}$ and $\cos\theta_{\rm decay}$ in the selection of $e^+e^- \to 5\pi$ are varied at all energy points. The largest difference of the cross section with respect to the nominal result at each energy point is taken as the deviation of each requirement. The weighted-average deviation (with weights of statistics of each energy point) of each item is taken as the uncertainties. The uncertainties of $\cos\theta$, E/p, $|\Delta T|$, $p_{\mu^\pm}$, $M^{\eta}_{\pi^+\pi^-\gamma\gamma}$ and $\cos\theta_{\rm decay}$ are determined as 0.16%, 0.09%, 0.05%, 0.26%, 0.04%, and 0.40%, respectively. The uncertainties of the requirement of $\cos\theta_{\rm decay}$ are the same for the processes of $e^+e^- \to 5\pi$ and $e^+e^- \to \eta\pi^+\pi^-$.

The uncertainties associated with the fit procedure on the $M_{\gamma\gamma}$ and $M^{\eta}_{\pi^+\pi^-\gamma\gamma}$ distributions are estimated by changing the signal shapes to the Crystal Ball function and MC simulated histograms, respectively, extending or shrinking the fit ranges, changing the background shapes to a higher or lower order of the polynomial functions, and changing the interval width of each spectrum. The largest deviations of results for the different fit scenarios with respect to the nominal values are regarded as the individual systematic uncertainties and are added in quadrature to be the systematic uncertainty associated with the fit procedure. Due to the low statistics in the process of $e^+e^- \to \eta\pi^+\pi^-$, ensembles of simulated data samples (toy MC samples) at each energy point are generated according to the nominal fit result with the same statistics as data, then fitted by the alternative fitting scenario. These trials are performed 1000 times, and the average signal yields are taken as the results. For the data with the CM energy being 3101.92, 3106.14, 3112.62, and 3120.44 MeV, the statistics are extremely low and the uncertainties of the fit procedure are assigned to be the same as that for data at CM energy of 3099.61 MeV. Totally, the fit procedure introduces systematic uncertainties of about $1-2\%$ and 11% for the channels $e^+e^- \to 5\pi$ and $\eta\pi^+\pi^-$, respectively.

The systematic uncertainty due to the intermediate states in $e^+e^- \to \eta\pi^+\pi^-$ is about 3.0%, estimated as the difference between the weighted-average efficiency which takes into account the efficiencies and the relative branching fractions of $J/\psi \to \eta\pi^+\pi^-$ and $J/\psi \to \eta\rho^0$ and the efficiency of $J/\psi \to \eta\pi^+\pi^-$.

The uncertainty associated with $\epsilon_i^{\rm com}$ in the decay $e^+e^- \to 5\pi$ mainly comes from the statistical uncertainty of the relative ratios among different processes. Besides, the measured angular distributions of the pions in the MC samples are corrected to be the same as those measured in data. The systematic uncertainty due to the correction is estimated to be 0.1%-5.8% depending on the statistics of each dataset. The uncertainty of the luminosity determination is determined to be 1.1-1.3%, as listed in Table 1.

All the systematic uncertainties discussed above are combined in quadrature to obtain the overall systematic uncertainties.

4. Results

Due to the effects of radiation and CM energy spread, the observed cross section cannot be directly compared with the Born

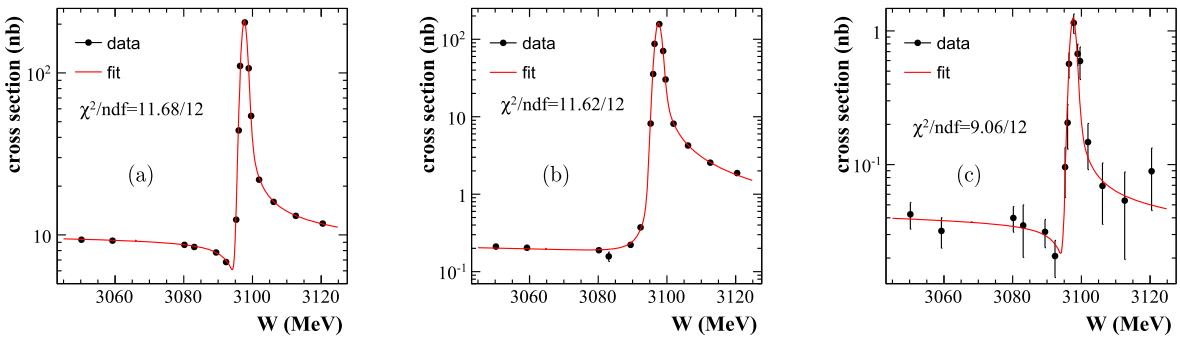

Fig. 3. The lineshapes of e^+e^- annihilates to (a) $\mu^+\mu^-$, (b) 5π, and (c) $\eta\pi^+\pi^-$. The black points with error bars are data, and the solid lines show the fit results.

cross section. In this section, the fit formulas for the observed cross section and fit results are presented.

The Born cross section of $e^+e^- \to \mu^+\mu^-$, consisting of only the pure EM contributions, A_γ and $A_{\rm cont}$, is conventionally expressed as [16–19]:

$$\sigma^0(W) = \frac{4\pi\alpha^2}{W^2}\left|1+\frac{3W^2\sqrt{\Gamma_{ee}\Gamma_{\mu\mu}}e^{i\Phi_{\gamma,\rm cont}}}{\alpha M(W^2-M^2+iM\Gamma)}\right|^2,$$

where α is the fine structure constant, M and Γ are the mass and width of the J/ψ, and Γ_{ee} and $\Gamma_{\mu\mu}$ are the partial widths of $J/\psi \to e^+e^-$ and $\mu^+\mu^-$, respectively. Incorporating the radiative correction $F(x,W)$, the cross section reads:

$$\sigma'(W) = \int_0^{1-(\frac{W_{\rm min}}{W})^2} dx F(x,W)\sigma^0(W\sqrt{1-x}),$$

where $W_{\rm min}$ is the minimum invariant mass of the $\mu^+\mu^-$ system, $x=\frac{2E_\gamma}{\sqrt{s}}$, E_γ is the energy of the radiation photon, and $F(x,W)$ is approximated as [36]:

$$F(x,W) = x^{\beta-1}\beta\cdot(1+\delta) - \beta(1-\frac{x}{2}) + \frac{1}{8}\beta^2\Big[4(2-x)\ln\frac{1}{x} - \frac{1+3(1-x)^2}{x}\ln(1-x) - 6 + x\Big],$$

with $\delta = \frac{3}{4}\beta + \frac{\alpha}{\pi}(\frac{\pi^2}{3}-\frac{1}{2}) + \beta^2(\frac{9}{32}-\frac{\pi^2}{12})$ and $\beta = \frac{2\alpha}{\pi}(2\ln\frac{W}{m_e}-1)$. The CM energy spread ($S_E$) is included by convolving with a Gaussian function with a width of S_E, and the expected cross section $\sigma''(W_i)$ at W_i is obtained as

$$\sigma''(W) = \int_{W-nS_E}^{W+nS_E}\frac{1}{\sqrt{2\pi}S_E}\exp\left(\frac{-(W-W')^2}{2S_E^2}\right)\sigma'(W')dW'.$$

Finally, the minimizing function is built with the factored minimization method separating the correlated and uncorrelated systematic uncertainties, and the effective variance-weighted least squares method [37] including the uncertainty ΔW along the X-axis by projecting it along the Y-axis. The resulting χ^2 reads

$$\chi^2 = \sum_{i=1}^{16}\frac{\left[\sigma_i^{\rm obs} - f\sigma''(W_i)\right]^2}{(\Delta\sigma_i^{\rm obs})^2 + \left[\Delta W_i\cdot\frac{d\sigma''(W)}{dW}\right]^2} + \left(\frac{1-f}{\Delta f}\right)^2,$$

where f is the normalization factor, and Δf is its uncertainty and set as the total correlated systematic uncertainty. The term $\Delta\sigma_i^{\rm obs}$ is the combined statistical and uncorrelated systematic uncertainties. Thus, the obtained uncertainties of results in this section include statistical and systematic ones. To be more efficient in the fitting procedure, instead of two integrations, an approximation [38–40] is used for $\sigma'(W)$, which is decomposed into a resonance and interference term $\sigma^{\rm R+I}(W)$ as well as a continuum term $\sigma^{\rm C}(W)$. The formulas can be found in the Appendix. The vacuum polarization is included by quoting the value of Γ_{ee}, $\Gamma_{\mu\mu}$ and Γ from the world averaged values [29,41].

We perform the minimized χ^2 fit to the measured cross section of $e^+e^- \to \mu^+\mu^-$ with the free parameters S_E, M, and $\Phi_{\gamma,\rm cont}$ and the fit curve is presented in Fig. 3 (a). The minimization gives $\Phi_{\gamma,\rm cont} = (3.0\pm5.7)^\circ$, which is consistent with zero as expected. A scan of the parameter $\Phi_{\gamma,\rm cont}$ in the full range $(-180^\circ, 180^\circ)$ confirms that only one solution exists. By further fixing the parameter $\Phi_{\gamma,\rm cont}$ to be zero, an alternative fit is carried out, resulting in values of S_E and M consistent with the previous fit. The resultant M is higher than its world average value $M_{J/\psi}$ [29], and indicates a deviation of the absolute energy calibration for the BEMS. Therefore, to obtain the proper detection efficiencies, the CM energies of MC samples are corrected by shifting the absolute values with $\Delta M = M - M_{J/\psi}$. To estimate the effect of fixed Γ_{ee}, $\Gamma_{\mu\mu}$ and Γ in the fit, the alternative fits are performed by letting these variables free in the fit. We also perform two additional fits, one with an alternative analytical formula in Ref. [18] which takes a different approximation, and the other is without the factored minimization method, in which the $\Delta\sigma_i^{\rm obs}$ is the statistical and systematic uncertainties added in quadrature. All of the results from various fits turn out to be consistent with each other. Taking into account the differences among different approaches and parameterizations, we obtain $\Phi_{\gamma,\rm cont} = (3.0\pm10.0)^\circ$, $S_E = (0.90\pm0.03)$ MeV and $\Delta M = (0.57\pm0.05)$ MeV/c^2, which will be used in the fit for the hadronic final state.

By assuming the $\Phi_{\gamma,\rm cont}$ to be zero, the Born cross section for $e^+e^- \to 5\pi$ is written as

$$\sigma^0(W) = \left(\frac{\mathcal{A}}{W^2}\right)^2\frac{4\pi\alpha^2}{W^2}\left|1+\frac{3W^2\sqrt{\Gamma_{ee}\Gamma_{\mu\mu}}(1+\mathcal{C}e^{i\Phi_{g,\rm EM}})}{\alpha M(W^2-M^2+iM\Gamma)}\right|^2,$$

where $\mathcal{C}$ is the ratio of $\frac{|A_g|}{|A_\gamma|}$, $\frac{\mathcal{A}}{W^2}$ is the form factor, and $\mathcal{A}$ is a free parameter in the fits. The decay width of $J/\psi \to 5\pi$ can be calculated as $\Gamma_{5\pi} = (\frac{\mathcal{A}}{W^2})^2\Gamma_{\mu\mu}|\mathcal{C}e^{i\Phi_{g,\rm EM}}+1|^2$, and the corresponding branching fraction is then $\mathcal{B}(J/\psi\to5\pi) = \Gamma_{5\pi}/\Gamma$. The analytical form $\sigma'(W)$ for the $e^+e^- \to 5\pi$ is similar to that for $e^+e^- \to \mu^+\mu^-$ (see Appendix). Similar to the fit for $e^+e^- \to \mu^+\mu^-$, we fix the parameters Γ_{ee}, $\Gamma_{\mu\mu}$ and Γ to the world average values [29] in the fit. By further fixing the values of M and S_E obtained in $e^+e^- \to \mu^+\mu^-$ and constraining $\Phi_{g,\rm EM}$ to be within $(0,180)^\circ$, the minimization fit yields $\Phi_{g,\rm EM} = (84.9\pm2.6)^\circ$ and $\mathcal{B}(J/\psi\to5\pi) = (4.73\pm0.41)\%$. An alternative fit with M and S_E

Table 3
Fit results for the lineshape of $e^+e^- \to 5\pi$. Solution I is with $\Phi_{g,\mathrm{EM}} > 0^\circ$ and solution II is with $\Phi_{g,\mathrm{EM}} < 0^\circ$.

	$\Phi_{g,\mathrm{EM}}$	$\mathcal{B}_{5\pi}$ (%)	χ^2/ndf
Solution I	$(84.9 \pm 3.6)^\circ$	4.73 ± 0.44	11.62/12
Solution II	$(-84.7 \pm 3.1)^\circ$	4.85 ± 0.45	11.62/12

being free parameters is performed to estimate the systematic uncertainty associated with the fixed M and S_E. The uncertainties associated with those of Γ_{ee}, $\Gamma_{\mu\mu}$ and Γ are evaluated by shifting the corresponding values within one standard deviation. The impact of f_i^{EC} is estimated by fitting the cross sections without incorporating it. The minimization function without the factor f is also applied to consider its influence. All results of $\Phi_{g,\mathrm{EM}}$ and $\mathcal{B}(J/\psi \to 5\pi)$ are consistent within the uncertainty and the differences are included into the final uncertainties which listed in Table 3.

Constraining $\Phi_{g,\mathrm{EM}}$ in the interval $(-180, 0)^\circ$, the second solution is found. The similar alternative fits described above are also carried out to estimate the corresponding systematic uncertainties. The results are listed in Table 3, too. As a check, the branching ratio of $J/\psi \to 5\pi$ *via* only A_γ can be calculated by $\mathcal{B}(J/\psi \to 5\pi)\frac{1}{|1+\mathcal{C}|^2}$, and it is consistent with the result calculated from $\mathcal{B}(J/\psi \to \mu^+\mu^-)\frac{\sigma(e^+e^-\to 5\pi)}{\sigma(e^+e^-\to\mu^+\mu^-)}$ within uncertainty.

The process $e^+e^- \to \eta\pi^+\pi^-$ is dominated by $e^+e^- \to \eta\rho^0$ (where the ρ^0 mixes with the ω), while the non-resonant $e^+e^- \to \eta\pi^+\pi^-$ decay is much smaller. Due to the limited statistics, the non-resonant decay is not considered in the fitting formula. The process with a ρ^0 intermediate state violates G parity and is therefore a pure EM process, while that with an ω intermediate state can also proceed through the strong interaction. Thus, the Born cross section for $\eta\pi^+\pi^-$ can be written as

$$\sigma^0(W) = \left(\frac{\mathcal{A}}{W^2}\right)^2 \frac{4\pi\alpha^2}{W^2} \times \left|1 + \frac{3W^2\sqrt{\Gamma_{ee}\Gamma_{\mu\mu}}\mathcal{C}_1 e^{i\Phi_{\gamma,\mathrm{cont}}}(1+\mathcal{C}_2 e^{i\Phi})}{\alpha M(W^2 - M^2 + iM\Gamma)}\right|^2,$$

where $\mathcal{C}_1$ represents the contribution from $e^+e^- \to \eta\rho^0$, and $\mathcal{C}_2$ and Φ are the ratio and the relative phase between the processes $J/\psi \to \eta\omega$ and $J/\psi \to \eta\rho^0$, respectively. The ratio between the branching fractions $\frac{\mathcal{B}(J/\psi\to\eta\omega,\omega\to\pi^+\pi^-)}{\mathcal{B}(J/\psi\to\eta\rho^0,\rho^0\to\pi^+\pi^-)}$ is $(0.138^{+0.025}_{-0.026})$ according to PDG [29]. Thus, $\mathcal{C}_2$ is fixed to be $\sqrt{0.138}$ in the fit. The branching fraction of $J/\psi \to \eta\pi^+\pi^-$ is determined by $(\frac{\mathcal{A}}{W^2})^2|\mathcal{C}_1 e^{i\Phi_{\gamma,\mathrm{cont}}}(1+\mathcal{C}_2 e^{i\Phi})|^2\mathcal{B}(J/\psi \to \mu^+\mu^-)$. Analogously, fixing the Γ_{ee}, $\Gamma_{\mu^+\mu^-}$ and Γ as well as M and S_E, and assuming the relative phase Φ to be 0° or 90° for two extreme cases since it cannot be extracted from the fit, the fit yields $\Phi_{\gamma,\mathrm{cont}}$ to be $(-2 \pm 36)^\circ$ or $(-22 \pm 36)^\circ$ with the same goodness of fit. The fit curve with $\Phi = 0^\circ$ is shown in Fig. 3 (c), where the lineshape of $e^+e^- \to \eta\pi^+\pi^-$ is very similar to that of the process $e^+e^- \to \mu^+\mu^-$, but different from that of $e^+e^- \to 5\pi$. The branching fractions in the two cases are both calculated to be $(3.78 \pm 0.66) \times 10^{-4}$. In alternative fits with floating M and S_E, changing Γ_{ee}, $\Gamma_{\mu^+\mu^-}$, Γ and $\mathcal{C}_2$ by one standard deviation, or using the minimization method without the factor f, neither the phase nor the branching fraction changes. Taking differences of various fit results as the systematic uncertainties, the phase $\Phi_{\gamma,\mathrm{cont}}$ is determined to be $(-2 \pm 36)^\circ$ or $(-22 \pm 36)^\circ$, and the $\mathcal{B}(J/\psi \to \eta\pi^+\pi^-)$ is $(3.78 \pm 0.68) \times 10^{-4}$.

5. Summary

For the first time, the relative phase between strong and EM amplitudes is measured directly from the J/ψ lineshape. Our result $\Phi_{g,\mathrm{EM}}$ being $(84.9 \pm 3.6)^\circ$ or $(-84.7 \pm 3.1)^\circ$ from the $e^+e^- \to 5\pi$ channel confirms the orthogonality between the strong and EM amplitudes and supports the hypothesis of a universal phase in J/ψ decays. The relative phase between EM amplitudes from J/ψ decays and from a virtual photon production in e^+e^- interactions, $\Phi_{\gamma,\mathrm{cont}}$ is determined from the $\mu^+\mu^-$ and $\eta\pi^+\pi^-$ processes, and the results are consistent with the zero-phase ansatz. Excluding the contribution from the continuum process and the interference, the branching fraction of J/ψ decays to 5π is measured to be $(4.73 \pm 0.44)\%$ or $(4.85 \pm 0.45)\%$, which is consistent with the world average value of $(4.1 \pm 0.5)\%$ [29]. The branching fraction of $J/\psi \to \eta\pi^+\pi^-$ is $(3.78 \pm 0.68) \times 10^{-4}$, which is more accurate than the existing world average value of $(4.0 \pm 1.7) \times 10^{-4}$ [29]. All the uncertainties of the results are the statistical and systematic uncertainties added in quadrature.

Acknowledgements

We thank the authors of the BABAYAGA and MCGPJ generators for their kind help and constructive discussion. The BESIII collaboration thanks the staff of BEPCII and the IHEP computing center for their strong support. This work is supported in part by Ministry of Science and Technology of China on the joined China-Italian project under Contract No. 2015DFG02380, National Key Basic Research Program of China under Contract No. 2015CB856700, 2015NSFC11375206; National Natural Science Foundation of China (NSFC) under Contracts Nos. 11235011, 11335008, 11425524, 11625523, 11635010; the Chinese Academy of Sciences (CAS) Large-Scale Scientific Facility Program; the CAS Center for Excellence in Particle Physics (CCEPP); Joint Large-Scale Scientific Facility Funds of the NSFC and CAS under Contracts Nos. U1332201, U1532257, U1532258; CAS under Contracts Nos. KJCX2-YW-N29, KJCX2-YW-N45; CAS Key Research Program of Frontier Sciences under Contracts Nos. QYZDJ-SSW-SLH003, QYZDJ-SSW-SLH040; 100 Talents Program of CAS; National 1000 Talents Program of China; INPAC and Shanghai Key Laboratory for Particle Physics and Cosmology; German Research Foundation DFG under Contracts Nos. Collaborative Research Center CRC 1044, FOR 2359; Istituto Nazionale di Fisica Nucleare, Italy; Koninklijke Nederlandse Akademie van Wetenschappen (KNAW) under Contract No. 530-4CDP03; Ministry of Development of Turkey under Contract No. DPT2006K-120470; National Natural Science Foundation of China (NSFC) under Contracts Nos. 11505034, 11575077; National Science and Technology fund; The Swedish Research Council; U. S. Department of Energy under Contracts Nos. DE-FG02-05ER41374, DE-SC-0010118, DE-SC-0010504, DE-SC-0012069; University of Groningen (RuG) and the Helmholtzzentrum fuer Schwerionenforschung GmbH (GSI), Darmstadt; WCU Program of National Research Foundation of Korea under Contract No. R32-2008-000-10155-0.

Appendix A. Analytical formula of radiation corrected cross section

The details of the deduction of the analytical formula of $e^+e^- \to \mu^+\mu^-$ around J/ψ has been published in Ref. [38–40]. Here, only the final formulas are presented. The continuum cross section after efficiency correction f_i^{EC} can be approximately written as:

$$\sigma^{C} = \frac{A}{W^2}\Big[1 + \frac{\beta}{2}(2\ln X_f - \ln(1-X_f) + \frac{3}{2} - X_f) + \frac{\alpha}{\pi}(\frac{\pi^2}{3} - \frac{1}{2})\Big].$$

The resonance and interference part is:

$$\begin{aligned}\sigma^{R+I}(W) = C_1(1+\delta)\cdot\Bigg[&a^{\beta-2}\varphi(\cos\zeta,\beta) + \beta(\frac{X_f^{\beta-2}}{\beta-2} + \frac{X_f^{\beta-3}}{\beta-3}R_2 + \frac{X_f^{\beta-4}}{\beta-4}R_3)\Bigg]\\ &+\Big[-\beta(1+\delta)C_2 + (-\beta - \frac{\beta^2}{4})C_1\Big]\\ &\cdot\Bigg[\frac{a^{\beta-1}}{1+\beta}\varphi(\cos\zeta,\beta+1) + \frac{X_f^{\beta-1}}{\beta-1} + \frac{X_f^{\beta-2}}{\beta-2}R_2 + \frac{X_f^{\beta-3}}{\beta-3}R_3\Bigg]\\ &+\Bigg[\frac{1}{2}\ln\frac{X_f^2 + 2aX_f\cos\zeta + a^2}{a^2} - \mathrm{ctg}\zeta(\mathrm{tg}^{-1}\frac{X_f + a\cos\zeta}{a\sin\zeta} - \frac{\pi}{2} + \zeta)\Bigg]\\ &\cdot\Big[(\beta + \frac{\beta^2}{4})\cdot C_2 + (\frac{\beta}{2} - \frac{3}{8}\beta^2)\cdot C_1\Big].\end{aligned}$$

Here $a^2 = (1 - \frac{M^2}{W^2})^2 + \frac{M^2\Gamma^2}{W^4}$, $\cos\zeta = \frac{1}{a}(\frac{M^2}{W^2} - 1)$, $\varphi(\cos\zeta, y) = \frac{\pi y \sin[\zeta(1-y)]}{\sin\zeta\sin\pi y}$, $R_2 = \frac{2(W^2-M^2)}{W^2} = -2a\cos\zeta$, $R_3 = a^2(4\cos^2\zeta - 1)$, $X_f = 1 - \frac{W^2_{\min}}{W^2}$. For $e^+e^- \to \mu^+\mu^-$, C_1 and C_2 are:

$$\begin{aligned}C_1 &= \Bigg\{8\pi\alpha^2\frac{\sqrt{\Gamma_{ee}\Gamma_{\mu\mu}}}{M}\Big[(W^2 - M^2)\cos\Phi_{\gamma,\mathrm{cont}} + \sin\Phi_{\gamma,\mathrm{cont}}M\Gamma\Big] + \frac{12\pi\Gamma_{ee}\Gamma_{\mu\mu}}{M^2}W^2\Bigg\}/W^4,\\ C_2 &= \Bigg[\frac{8\pi\alpha\sqrt{\Gamma_{ee}\Gamma_{\mu\mu}}}{M}\cos\Phi_{\gamma,\mathrm{cont}} + \frac{12\pi\Gamma_{ee}\Gamma_{\mu\mu}}{M^2}\Bigg]/W^2.\end{aligned}$$

For $e^+e^- \to 5\pi$, the analytical formula is very similar to $e^+e^- \to \mu^+\mu^-$, but the C_1 and C_2 are changed as:

$$\begin{aligned}C_1 = \{&8\pi\alpha^2\frac{\sqrt{\Gamma_{ee}\Gamma_{\mu\mu}}}{M}\Big[(W^2 - M^2)(\mathcal{C}\cos\Phi_{g,\mathrm{EM}} + 1) + \mathcal{C}\sin\Phi_{g,\mathrm{EM}}M\Gamma\Big]\\ &+ \frac{12\pi\Gamma_{ee}\Gamma_{\mu\mu}}{M^2}W^2(1 + \mathcal{C}^2 + 2\mathcal{C}\cos\Phi_{g,\mathrm{EM}})\}/W^4,\\ C_2 = \Bigg[&\frac{8\pi\alpha\sqrt{\Gamma_{ee}\Gamma_{\mu\mu}}}{M}(\mathcal{C}\cos\Phi_{g,\mathrm{EM}} + 1)\\ &- \frac{12\pi\Gamma_{ee}\Gamma_{\mu\mu}}{M^2}(1 + \mathcal{C}^2 + 2\mathcal{C}\cos\Phi_{g,\mathrm{EM}})\Bigg]/W^2.\end{aligned}$$

For $\eta\pi^+\pi^-$, the corresponding C_1 and C_2 are changed to

$$\begin{aligned}C_1 = \{&8\pi\alpha^2\frac{\sqrt{\Gamma_{ee}\Gamma_{\mu\mu}}}{M}[(W^2 - M^2)\mathcal{C}_1(\cos\Phi_{\gamma,\mathrm{cont}} + \mathcal{C}_2\cos\Phi_{\gamma,\mathrm{cont}}\cos\Phi - \mathcal{C}_2\sin\Phi_{\gamma,\mathrm{cont}}\sin\Phi)\\ &+ M\Gamma\mathcal{C}_1(\sin\Phi_{\gamma,\mathrm{cont}} + \mathcal{C}_2\sin\Phi_{\gamma,\mathrm{cont}}\cos\Phi + \mathcal{C}_2\cos\Phi_{\gamma,\mathrm{cont}}\sin\Phi)]\\ &+ \frac{12\pi\Gamma_{ee}\Gamma_{\mu\mu}}{M^2}W^2\mathcal{C}_1^2(1 + \mathcal{C}_2^2 + 2\mathcal{C}_2\cos\Phi)\}/W^4,\\ C_2 = [&\frac{8\pi\alpha\sqrt{\Gamma_{ee}\Gamma_{\mu\mu}}}{M}\mathcal{C}_1(\cos\Phi_{\gamma,\mathrm{cont}} + \mathcal{C}_2\cos\Phi_{\gamma,\mathrm{cont}}\cos\Phi - \mathcal{C}_2\sin\Phi_{\gamma,\mathrm{cont}}\sin\Phi)\\ &+ \frac{12\pi\Gamma_{ee}\Gamma_{\mu\mu}}{M^2}\mathcal{C}_1^2(1 + \mathcal{C}_2^2 + 2\mathcal{C}_2\cos\Phi)]/W^2.\end{aligned}$$

References

[1] S.J. Brodsky, G.P. Lepage, S.F. Tuan, Phys. Rev. Lett. 59 (1987) 621.
[2] V.L. Chernyak, I.R. Zhinitski, Nucl. Phys. B 246 (1984) 52.
[3] J. Jousset, et al., DMII collaboration, Phys. Rev. D 41 (1990) 1389.
[4] D. Coffman, et al., Mark III collaboration, Phys. Rev. D 38 (1988) 2695.
[5] M. Suzuki, Phys. Rev. D 60 (1999) 051501.
[6] G.L. Castro, J.L. Lucio M., J. Pestieau, AIP Conf. Proc. 342 (1995) 441.
[7] L. Köpke, N. Wermes, Phys. Rep. 174 (1989) 67.
[8] M. Suzuki, Phys. Rev. D 63 (2001) 054021.
[9] R. Baldini, et al., Phys. Lett. B 444 (1998) 111.
[10] K. Zhu, X.H. Mo, C.Z. Yuan, Int. J. Mod. Phys. A 30 (2015) 1550148.
[11] Y.Q. Chen, E. Braaten, Phys. Rev. Lett. 80 (1998) 5060.
[12] M. Fukugita, J. Kwiecinski, Ruth. Lab. RL-79-45, 1979.
[13] W.S. Hou, A. Soni, Phys. Rev. Lett. 50 (1983) 569.
[14] P.G.O. Freund, Y. Nambu, Phys. Rev. Lett. 34 (1975) 1645.
[15] R. Baldini, C. Bini, E. Luppi, Phys. Lett. B 404 (1997) 362.
[16] A.M. Boyarski, et al., Phys. Rev. Lett. 34 (1975) 1357.
[17] J.Z. Bai, et al., BES Collaboration, Phys. Lett. B 355 (1995) 374.
[18] V.V. Anashin, et al., Phys. Lett. B 685 (2010) 134.
[19] F.A. Berends, R. Gastmans, Electromagnetic Interactions of Hadrons, Springer, New York, 1978.
[20] J.M. Gerard, J. Weyers, Phys. Lett. B 462 (1999) 324.
[21] M. Ablikim, et al., BESIII Collaboration, Nucl. Instrum. Methods A 614 (2010) 345.
[22] M. Ablikim, et al., BESIII Collaboration, Chin. Phys. C 41 (2017) 063001.
[23] E.V. Abakumova, et al., Nucl. Instrum. Methods A 659 (2011) 21.
[24] S. Agostinelli, et al., Geant4 Collaboration, Nucl. Instrum. Methods A 506 (2003) 250.
[25] C.M.C. Calame, G. Montagna, O. Nicrosini, F. Piccinini, arXiv:hep-ph/0312014.
[26] R.G. Ping, Chin. Phys. C 32 (2008) 599.
[27] D.J. Lange, Nucl. Instrum. Methods A 462 (2001) 152.
[28] A.B. Arbuzov, et al., Eur. Phys. J. C 46 (2006) 689.
[29] C. Patrignani, et al., Particle Data Group, Chin. Phys. C 40 (2016) 100001.
[30] J.C. Chen, et al., Phys. Rev. D 62 (2000) 034003.
[31] J.P. Lees, et al., BaBar Collaboration, Phys. Rev. D 86 (2012) 032013.
[32] B. Aubert, et al., BaBar Collaboration, Phys. Rev. D 73 (2006) 052003.
[33] W.L. Yuan, et al., Chin. Phys. C 40 (2016) 026201.
[34] V. Prasad, et al., Springer Proc. Phys. 174 (2016) 577.
[35] M. Ablikim, et al., BESIII Collaboration, Phys. Rev. D 83 (2011) 032003.
[36] E.A. Kuraev, V.S. Fadin, Sov. J. Nucl. Phys. 41 (1985) 466.
[37] B.P. Roe, Probability and Statistics in Experimental Physics, 2nd edn., Springer, New York, 2001.
[38] P. Wang, Y.S. Zhu, X.H. Mo, arXiv:0907.0734v1.
[39] F.Z. Chen, P. Wang, J.M. Wu, Y.S. Zhu, HEP & NP 14 (1990) 585.
[40] X.Y. Zhou, Y.D. Wang, L.G. Xia, Chin. Phys. C 41 (2017) 083001.
[41] J.P. Alexander, et al., Nucl. Phys. B 320 (1989) 45.